*R*esearch in
*A*stronomy and
*A*strophysics

The $Y_{\mathrm{SZ},Planck} - Y_{\mathrm{SZ},XMM}$ scaling relation and its difference between cool-core and non-cool-core clusters

Yue Zhu[1], Yuan-Hao Wang[1], Hai-Hui Zhao[2], Shu-Mei Jia[1], Cheng-Kui Li[1] and Yong Chen[1]

[1] Key Laboratory for Particle Astrophysics, Institute of High Energy Physics, Chinese Academy of Sciences, Beijing 100049, China; *ychen@ihep.ac.cn*

[2] Department of Physics and Institute of Theoretical Physics, Nanjing Normal University, Nanjing 210023, China

Abstract We construct a sample of 70 clusters using data from *XMM-Newton* and *Planck* to investigate the $Y_{\mathrm{SZ},Planck} - Y_{\mathrm{SZ},XMM}$ scaling relation and the cool-core influences on this relation. $Y_{\mathrm{SZ},XMM}$ is calculated by accurately de-projected temperature and electron number density profiles derived from *XMM-Newton*. $Y_{\mathrm{SZ},Planck}$ is the latest *Planck* data restricted to our precise X-ray cluster size θ_{500}. To study the cool-core influences on the $Y_{\mathrm{SZ},Planck} - Y_{\mathrm{SZ},XMM}$ scaling relation, we apply two criteria, namely the limits of central cooling time and classic mass deposition rate, to distinguish cool-core clusters (CCCs) from non-cool-core clusters (NCCCs). We also use $Y_{\mathrm{SZ},Planck}$ from other papers, which are derived from different methods, to confirm our results. The intercept and slope of the $Y_{\mathrm{SZ},Planck} - Y_{\mathrm{SZ},XMM}$ scaling relation are $A = -0.86 \pm 0.30$ and $B = 0.83 \pm 0.06$ respectively. The intrinsic scatter is $\sigma_{\mathrm{ins}} = 0.14 \pm 0.03$. The ratio of $Y_{\mathrm{SZ},Planck}/Y_{\mathrm{SZ},XMM}$ is 1.03 ± 0.05, which is in excellent statistical agreement with unity. Discrepancies in the $Y_{\mathrm{SZ},Planck} - Y_{\mathrm{SZ},XMM}$ scaling relation between CCCs and NCCCs are found in the observation. They are independent of the cool-core classification criteria and $Y_{\mathrm{SZ},Planck}$ calculation methods, although the discrepancies are more significant under the classification criteria of classic mass deposition rate. The intrinsic scatter of CCCs (0.04) is quite small compared to that of NCCCs (0.27). The ratio of $Y_{\mathrm{SZ},Planck}/Y_{\mathrm{SZ},XMM}$ for CCCs is 0.89 ± 0.05, suggesting that CCCs' $Y_{\mathrm{SZ},XMM}$ may overestimate the Sunyaev-Zel'dovich (SZ) signal. By contrast, the ratio of $Y_{\mathrm{SZ},Planck}/Y_{\mathrm{SZ},XMM}$ for NCCCs is 1.14 ± 0.12, which indicates that NCCCs' $Y_{\mathrm{SZ},XMM}$ may underestimate the SZ signal.

Key words: galaxies: clusters: intracluster medium — X-rays: galaxies: clusters — cosmology: observations

1 INTRODUCTION

Galaxy clusters are the largest gravitationally bound systems in the universe, formed by the collapse of matter under its self-gravity and the merging of smaller clusters (Colberg et al. 1999; Kravtsov & Borgani 2012). The process of formation is sensitive to the evolution of the universe, therefore the study of galaxy clusters can trace the growth of large-scale structure and constrain cosmological parameters (Seljak et al. 2006; Vikhlinin et al. 2009b; Mantz et al. 2010; Rozo et al. 2010; Benson et al. 2013; Planck Collaboration et al. 2014, 2016a). Cluster mass is the most important quantity when using clusters as cosmological probes. However, directly measuring cluster mass is difficult because about 87% of cluster mass is in the form of dark matter. Instead, we infer cluster mass through scaling relations with quantities that are convenient to observe, such as X-ray luminosity and temperature, velocity dispersion and flux from the thermal Sunyaev-Zel'dovich (tSZ) effect (Arnaud et al. 2005; Maughan 2007; Reichert et al. 2011; Zhang et al. 2011; Böhringer et al. 2013; Bocquet et al. 2015; Munari et al. 2013).

The tSZ effect (Sunyaev & Zeldovich 1980) describes a distortion of the cosmic microwave background (CMB) spectrum caused by inverse Compton scattering of CMB photons off hot gas in the intracluster medium (ICM). The integrated Compton parameter Y_{SZ} is acquired by integration of the tSZ signal over the cluster extent V, with the

temperature T_e and electron number density n_e, as

$$Y_{SZ} = D_A^{-2} \frac{k_B \sigma_T}{m_e c^2} \int n_e T_e dV = D_A^{-2} \frac{\sigma_T}{m_e c^2} \int P_e dV \,,$$

(1)

where P_e is the gas pressure, $P_e = n_e k_B T_e$, k_B is the Boltzmann constant, σ_T is the Thomson cross-section, $m_e c^2$ is the electron rest mass and D_A is the angular diameter distance. Kravtsov et al. (2006) introduce Y_{SZ}'s X-ray analog, Y_X, which is the product of the cluster X-ray temperature T_X and gas mass M_{gas}. Both Y_{SZ} and Y_X represent the total thermal energy of the cluster, therefore they are good mass proxies with low intrinsic scatter and with little relevance to the complicated dynamical state in clusters (Motl et al. 2005; Nagai 2006; Arnaud et al. 2007; Zhao et al. 2013; Mahdavi et al. 2013; Sembolini et al. 2014). We should note that to obtain the precise mass from the scaling relations, biases induced by the selection effects should be taken into account (Pratt et al. 2009; Allen et al. 2011; Angulo et al. 2012; Andersson et al. 2011). Y_{SZ} has already been applied to derive the cluster mass in some works, and serious consideration is given to possible bias in the mass proxy (Aghanim et al. 2009; Comis et al. 2011; Planck Collaboration et al. 2011c; Jimeno et al. 2018).

Y_{SZ} can be obtained by two methods: 1) direct Sunyaev-Zel'dovich (SZ) observation, $Y_{SZ,CMB}$; 2) the SZ signal based on ICM properties derived from X-ray observation, $Y_{SZ,X-ray}$. $Y_{SZ,CMB}$ is proportional to $n_e T_e$ and relies more on the region outside the cluster core, while $Y_{SZ,X-ray}$ is sensitive to clumping regions because the X-ray flux given by bremsstrahlung emission is proportional to $n_e^2 T_e^{1/2}$. The different dependences of SZ and X-ray observations on n_e and T_e may have an influence on the $Y_{SZ,CMB}$-$Y_{SZ,X-ray}$ relation due to various physical processes in clusters. Therefore, the comparison between $Y_{SZ,CMB}$ and $Y_{SZ,X-ray}$ may reveal discrepancies between cool-core clusters (CCCs) and non-cool-core clusters (NCCCs), increasing knowledge about the bias and intrinsic scatter in the SZ/X-ray scaling relation. Furthermore, unlike X-ray observation, SZ observation is not affected by surface brightness dimming, thus it is an ideal probe for galaxy clusters at high redshift. The SZ/X-ray scaling relation can be used to infer cluster mass, producing completive cosmology measurements.

Most previous works have focused on the relation between Y_{SZ} and Y_X. Normally, $Y_{SZ,CMB}$ is not distinguished from $Y_{SZ,X-ray}$. They are applied to study the $Y_{SZ,X-ray}$-Y_X scaling relation (Arnaud et al. 2010) and the $Y_{SZ,CMB}$-Y_X scaling relation, and researchers have ascertained that the two relations are consistent with each other (Andersson et al. 2011; Planck Collaboration et al. 2013a;

Rozo et al. 2014b,a; Biffi et al. 2014; Czakon et al. 2015). Several papers examine the $Y_{SZ,CMB} - Y_{SZ,X-ray}$ scaling relation (Bonamente et al. 2012; De Martino & Atrio-Barandela 2016), and also find good agreement between the SZ signal and its X-ray prediction. Additionally, the outskirts of NCCCs have rich substructures, while those of CCCs are more homogeneous and relaxed. However, no discrepancy has been identified between CCCs and NCCCs in observations so far (Planck Collaboration et al. 2011a; Rozo et al. 2012; De Martino & Atrio-Barandela 2016).

In the following, we use a sample of 70 clusters to determine the $Y_{SZ,CMB} - Y_{SZ,X-ray}$ scaling relation. Accurate ICM properties, derived from *XMM-Newton* data analyzed with the β model and the de-projected method, are applied to calculate $Y_{SZ,X-ray}$. On the other hand, $Y_{SZ,CMB}$ is obtained from the latest *Planck* catalog. Every quantity in our analysis, e.g., T_e and n_e, is directly derived from observations, independent of any assumed scaling relations which are widely used in other works to infer some quantities. This approach can reduce artificial correlations introduced in data processing and improve the reliability of our results.

The paper is organized as follows. In Section 2 we introduce the cluster sample and describe the SZ and X-ray data analysis. In Section 3 we investigate the $Y_{SZ,CMB} - Y_{SZ,X-ray}$ scaling relation and the influences of CCCs and NCCCs on this relation. Discussions about our results are also presented. We provide a conclusion in Section 4.

We assume a flat ΛCDM cosmology with $\Omega_M = 0.3$, $\Omega_\Lambda = 0.7$ and $H_0 = 70 \, \mathrm{km \, s^{-1} \, Mpc^{-1}}$. All uncertainties are quoted at the 68% confidence level.

2 DATA

2.1 Cluster Sample

Our sample is extracted from an *XMM-Newton* bright cluster sample (XBCS) (Zhao 2015; Zhao et al. 2015) and the *Planck* PSZ2 catalog (Planck Collaboration et al. 2016b). For the XBCS, we select clusters with a flux-limited ($f_X [0.1 - 2.4 \, \mathrm{keV}] \geq 1.0 \times 10^{-11} \, \mathrm{erg \, s^{-1} \, cm^{-2}}$) method from several cluster catalogs based on the *ROSAT* All-Sky Survey (RASS; De Grandi et al. 1999): HIghest X-ray FLUx Galaxy Cluster Sample (HIFLUGCS; Reiprich & Böhringer 2002), *ROSAT*-ESO Flux Limited X-ray catalog (REFLEX; Böhringer et al. 2004), Northern *ROSAT* Brightest Cluster Sample (NORAS; Böhringer et al. 2000), X-ray-bright Abell-type clusters (XBACs Ebeling et al. 1996) and *ROSAT* Brightest Cluster Sample (BCS; Ebeling

et al. 1998). Among the XBCS entries, 78 clusters are available in the PSZ2 catalog. The positions of the cluster centers identified by *XMM-Newton* and *Planck* exhibit some deviation. Clusters with conditions of $\Delta D > 4'$ or $\Delta D > 0.3R_{500}$ are excluded, where ΔD is the positional offset between two centers and the R_{500} is the cluster radius where the mean density is 500 times the critical density of the universe at the cluster redshift. Our final sample consists of 70 clusters, covering the redshift from about 0.01 to 0.25. The mass within R_{500} of these galaxy clusters ranges from 0.27 to 11.5 $\times 10^{14}\, M_\odot$, while the R_{500} ranges from 0.44 to 2.45 Mpc.

2.2 *Planck* Data

The PSZ2 catalog is constructed by blind detection over the full sky using three independent extraction algorithms: MMF1, MMF3 and PsW, with no prior positional information on known clusters. MMF1 and MMF3 are based on a matched-multi-frequency filter algorithm. PsW is a fast Bayesian multi-frequency algorithm. All three algorithms assume the generalized Navarro-Frenk-White (GNFW) pressure profile (Arnaud et al. 2010) as prior spatial characteristics for the cluster, given by

$$p(r) = \frac{P_0}{(c_{500}r/R_{500})^\gamma [1 + (c_{500}r/R_{500})^\alpha]^{(\beta-\gamma)/\alpha}} \quad (2)$$

with the parameters (Planck Collaboration et al. 2014)

$$[P_0, c_{500}, \gamma, \alpha, \beta] = [8.40h_{70}^{-3/2}, 1.177, 0.308, 1.05, 5.49],$$

where α, β and γ are the logarithmic slopes for the intermediate region ($c_{500}r \sim R_{500}$), the outer region ($c_{500}r \gg R_{500}$) and the core region ($c_{500}r \ll R_{500}$), respectively, c_{500} is the concentration parameter through which θ_{500} (instead of radial coordinates, angular coordinates are more often used, as $\theta_{500} = R_{500}/D_A$) is related to the characteristic cluster scale θ_s ($\theta_s = \theta_{500}/c_{500}$), and P_0 is the normalization factor. θ_s and P_0 are free parameters in this profile.

For each detected source, each algorithm provides an estimated position, signal-to-noise ratio (S/N) value, a two-dimensional joint probability distribution for θ_s and the integrated Compton parameter within $5\theta_{500}$, Y_{5R500} (see Planck Collaboration et al. 2016a, fig.16).

Y_{5R500} and θ_s are strongly correlated, and we adopt θ_{500}, or equivalently θ_s, which is accurately derived from *XMM-Newton* observation (see Sect. 2.3) to break the $Y_{5R500} - \theta_s$ degeneracy. Given the θ_s from X-ray, the expectation and standard deviation from the Y_{5R500} conditional distribution are derived as the value of Y_{5R500}

and its uncertainty respectively. Uncertainties less than $0.05Y_{5R500}$ would be assigned to the standard deviation of Y_{5R500} in PSZ2, because they may be slightly underestimated by such Y_{5R500} estimation (Planck Collaboration et al. 2016b). Finally, Y_{500}, denoted as $Y_{SZ,Planck}$, is converted from Y_{5R500} by $Y_{5R500} = 1.79 \cdot Y_{500}$ for the pressure profile mentioned above (Arnaud et al. 2010; Planck Collaboration et al. 2014).

2.3 *XMM-Newton* Data

The XBCS is built using a flux-limited method. We process the *XMM-Newton* data of the whole cluster sample in a complicated way. Here only a brief description of the *XMM-Newton* data process is presented, and more details can be referred to in Zhao et al. (2013, 2015). *XMM-Newton* pn/EPIC data acquired in extended full frame mode or full frame mode are analyzed with Science Analysis System (SAS) 12.6.0. We select events with FLAG= 0 and PATTERN≤4, in which contaminated time intervals are discarded. Then we correct vignetting effects and out-of-time events, remove prominent background flares and point sources, and subtract the particle background and the cosmic X-ray background. After that, the cluster region is divided into several rings centered on the X-ray emission peak, with the width of the rings depending on the net photon counts. The point spread function (PSF, pn: FWHM = $6''$; XMM-Newton Users Handbook 2018) effect can be ignored because the minimum width of rings is set at $30''$. By subtracting all the contributions from the outer regions, the de-projected spectrum of each ring is obtained (Chen et al. 2003, 2007; Jia et al. 2004, 2006).

XSPEC version 12.8.1 is used for spectral analysis. The de-projected temperature T_e, metallicity and normalizing constant *norm* at each ring are derived from the de-projected spectral fits with the thermal plasma emission model Mekal (Mewe et al. 1985) and Wabs model (Morrison & McCammon 1983). Fitting the simulated spectrum using T_e and abundance profiles in XSPEC, one can get the de-projected electron number density n_e at each ring.

Limited by the *XMM-Newton* field of view and the statistics of photons from clusters, the maximum observable radius of clusters, R_{max}, is usually smaller than R_{500}. In the case of $R_{max} < R_{500}$, T_e at $r > R_{max}$ is set to the same value in the outermost ring. Linear interpolation is used to calculate $T_e(r)$. For the fits of electron density profile $n_e(r)$, the single β model and double β model are both adopted.

Table 1 $Y_{\mathrm{SZ},Planck} - Y_{\mathrm{SZ},XMM}$ Scaling Relations for Five Samples

Sample	N	A	B	σ_{ins}	$Y_{\mathrm{SZ},Planck}/Y_{\mathrm{SZ},XMM}$*	$\sigma_{\mathrm{ins}\,|\,B=1}$
MMF1	67	-0.79 ± 0.36	0.80 ± 0.07	0.20 ± 0.04	1.27 ± 0.08	0.22 ± 0.05
MMF3	66	-0.80 ± 0.26	0.85 ± 0.05	0.10 ± 0.03	0.95 ± 0.05	0.11 ± 0.03
PsW	61	-0.99 ± 0.28	0.82 ± 0.05	0.11 ± 0.03	0.93 ± 0.05	0.13 ± 0.03
MaxSN	[a]70	-1.11 ± 0.31	0.77 ± 0.06	0.17 ± 0.04	1.07 ± 0.06	0.20 ± 0.04
NEAREST	[b]70	-0.86 ± 0.30	0.83 ± 0.06	0.14 ± 0.03	1.03 ± 0.05	0.15 ± 0.04

Notes: The cluster number contributed by each algorithm to the MaxSN and NEAREST samples: [a] MMF1: 16, MMF3: 29, PsW: 25; [b] MMF1: 18, MMF3: 18, PsW: 34; * $Y_{\mathrm{SZ},Planck}/Y_{\mathrm{SZ},XMM} = 10^{A\,|\,B=1}$.

Table 2 $Y_{\mathrm{SZ},Planck} - Y_{\mathrm{SZ},XMM}$ Scaling Relations for CCCs and NCCCs in the NEAREST Subsample with Two Cool-core Classification Criteria

Class.	Sample	N	A	B	σ_{ins}	$Y_{\mathrm{SZ},Planck}/Y_{\mathrm{SZ},XMM}$	$\sigma_{\mathrm{ins}\,|\,B=1}$
[a] Z13	NCCCs	28	-0.54 ± 0.49	0.88 ± 0.10	0.20 ± 0.07	1.09 ± 0.10	0.20 ± 0.07
	CCCs	27	-1.33 ± 0.52	0.74 ± 0.10	0.11 ± 0.04	0.97 ± 0.08	0.13 ± 0.05
[b] C07	NCCCs	29	-0.84 ± 0.57	0.81 ± 0.11	0.27 ± 0.09	1.14 ± 0.12	0.28 ± 0.09
	CCCs	26	-0.78 ± 0.36	0.86 ± 0.07	0.04 ± 0.02	0.89 ± 0.05	0.04 ± 0.02

Notes: [a] Zhao et al. (2013); [b] Chen et al. (2007).
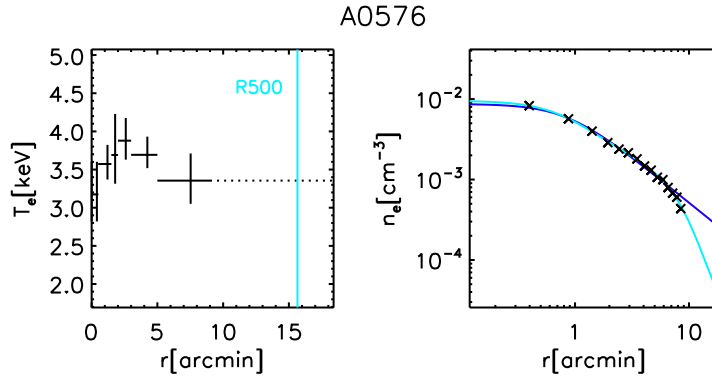
Fig. 1 Illustration of profiles for cluster A0576. Left panel: temperature with error bar at each ring. A *light blue vertical line* indicates the position of R_{500}. Extrapolation of temperature is shown as a *dotted line*. Right panel: electron number density (marked as *cross symbols*) at each ring. A *light blue line* and *deep blue line* indicate the density profiles fitting by the single β model and double β model, respectively.

The single β model gives

$$n_{\mathrm{e}}(r) = n_0 \left[1 + \left(\frac{r}{r_{\mathrm{c}}} \right)^2 \right]^{-\frac{3}{2}\beta}, \tag{3}$$

where n_0 is the electron number density and r_{c} is the core radius.

The double β model is in the form of

$$n_{\mathrm{e}}(r) = n_{01} \left[1 + \left(\frac{r}{r_{c1}} \right)^2 \right]^{-\frac{3}{2}\beta_1} + n_{02} \left[1 + \left(\frac{r}{r_{c2}} \right)^2 \right]^{-\frac{3}{2}\beta_2}, \tag{4}$$

where n_{01} and n_{02} are the electron number density, and r_{c1} and r_{c2} are the core radius for the inner and outer components respectively (Chen et al. 2003).

For most clusters, the double β model fits significantly better than the single β model, however for some clus-

ters, the improvements are negligible. As a result, 54 and 16 clusters are fitted with the double and single β model, respectively. Figure 1 shows a typical cluster profile. It clearly indicates that the double β model matches the electron number density data better than the single β model.

The influences of the center offsets ΔD between *XMM-Newton* observation and three *Planck* algorithm detections are considered. Because of the *Planck* blind detection, we cannot fix our X-ray cluster position to that provided by the *Planck* detection procedure and re-extract $Y_{\mathrm{SZ},Planck}$. Instead, we correct the $Y_{\mathrm{SZ},XMM}$ by changing its integral center. The cluster is assumed to be spherically
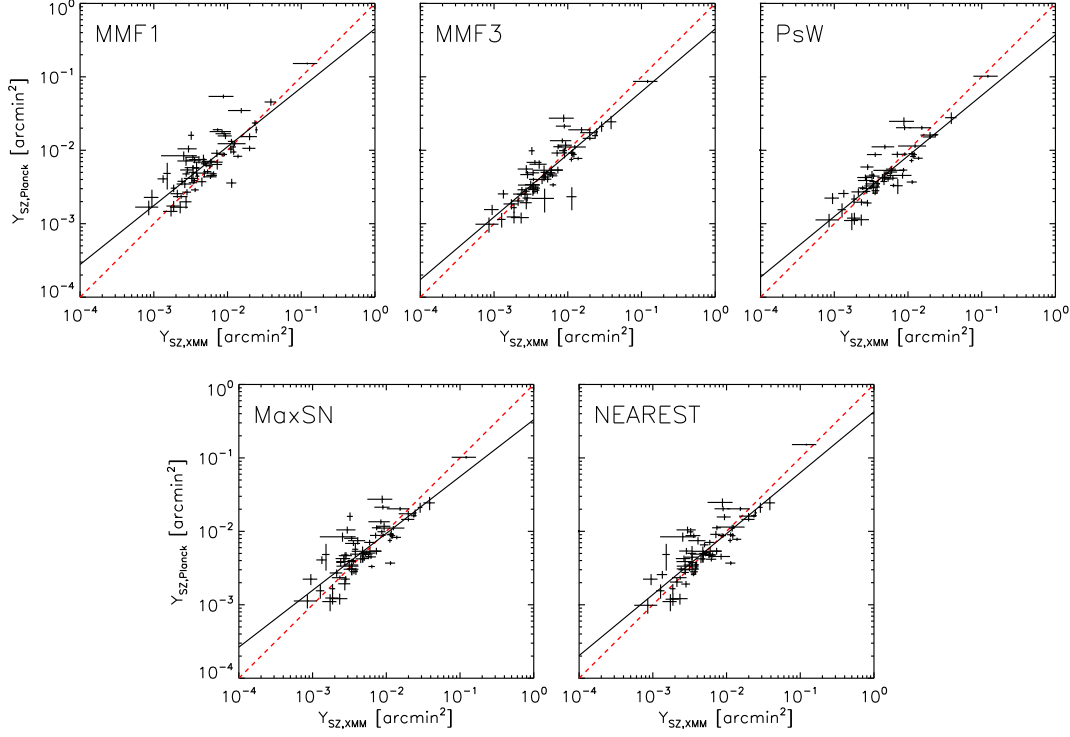
Fig. 2 Scaling relations between $Y_{\mathrm{SZ},XMM}$ and $Y_{\mathrm{SZ},Planck}$. $Y_{\mathrm{SZ},XMM}$ is modified by the cluster center differences between the X-ray results and the algorithms used to determine $Y_{\mathrm{SZ},Planck}$. Top panels: $Y_{\mathrm{SZ},Planck}$ is measured using MMF1, MMF3 and PsW algorithms, from left to right respectively. Bottom panels: combination of the three algorithms. Bottom left: $Y_{\mathrm{SZ},Planck}$ is determined by the most significant detection algorithm. Bottom right: $Y_{\mathrm{SZ},Planck}$ is assigned by the algorithm which gives the closest position from the X-ray center. The *solid black lines* represent the best fit lines and the *dashed red lines* show the relations of $X = Y$.
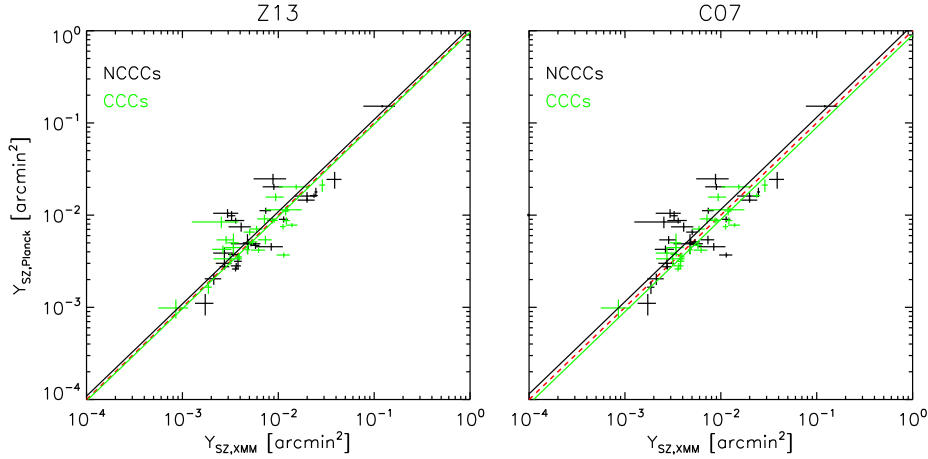
Fig. 3 $Y_{\mathrm{SZ},Planck} - Y_{\mathrm{SZ},XMM}$ scaling relations for CCCs and NCCCs in the NEAREST subsample. Z13 criteria (left, Zhao et al. 2013) and C07 criteria (right, Chen et al. 2007) on CCCs and NCCCs are shown. *Black dots* indicate NCCCs and *green dots* signify CCCs. The *black and green solid lines* are the best fit lines of $Y_{\mathrm{SZ},Planck}/Y_{\mathrm{SZ},XMM}$ for NCCCs and CCCs, respectively. The *dashed red lines* show the relations of $X = Y$.

symmetric, and $Y_{\mathrm{SZ},XMM}$ within R_{500} is given by

$$Y_{500} = D_{\mathrm{A}}^{-2} \frac{k_{\mathrm{B}}\sigma_{\mathrm{T}}}{m_{\mathrm{e}}c^2} \int_{-R_{500}+\Delta D}^{R_{500}+\Delta D} \int_{-R_y}^{R_y} \int_{-R_z}^{R_z} n_{\mathrm{e}}T_{\mathrm{e}} dx dy dz \;,$$

$$(5)$$

where $R_y = \sqrt{R_{500}^2 - x^2}$ and $R_z = \sqrt{R_{500}^2 - x^2 - y^2}$.

We adopt the Monte-Carlo method to estimate the uncertainties of $Y_{\mathrm{SZ},XMM}$. For each cluster, we simulate T_{e} at each shell, and the parameters of the β model for the n_{e}

Table 3 $Y_{\mathrm{SZ},Planck} - Y_{\mathrm{SZ},XMM}$ Scaling Relations for CCCs and NCCCs with Two Cool-core Classification Criteria

Sample	Class.	Sub-Sample	N	A	B	σ_{ins}	$Y_{\mathrm{SZ},Planck}/Y_{\mathrm{SZ},XMM}$	$\sigma_{\mathrm{ins}\,|\,B=1}$
MMF1	Z13	NCCCs	28	-0.32 ± 0.54	0.87 ± 0.11	0.28 ± 0.10	1.40 ± 0.15	0.28 ± 0.09
		CCCs	25	-1.71 ± 0.59	0.64 ± 0.12	0.12 ± 0.05	1.14 ± 0.10	0.16 ± 0.06
	C07	NCCCs	29	-0.62 ± 0.61	0.81 ± 0.12	0.34 ± 0.11	1.40 ± 0.17	0.35 ± 0.11
		CCCs	24	-0.93 ± 0.52	0.79 ± 0.10	0.08 ± 0.04	1.13 ± 0.08	0.09 ± 0.04
MMF3	Z13	NCCCs	26	-0.70 ± 0.46	0.84 ± 0.09	0.17 ± 0.06	1.08 ± 0.10	0.18 ± 0.07
		CCCs	26	-1.00 ± 0.40	0.83 ± 0.08	0.05 ± 0.03	0.87 ± 0.05	0.05 ± 0.03
	C07	NCCCs	27	-0.72 ± 0.51	0.85 ± 0.10	0.22 ± 0.09	1.03 ± 0.10	0.22 ± 0.08
		CCCs	25	-0.97 ± 0.36	0.83 ± 0.07	0.04 ± 0.02	0.88 ± 0.05	0.05 ± 0.02
PsW	Z13	NCCCs	24	-0.42 ± 0.45	0.92 ± 0.09	0.12 ± 0.06	0.99 ± 0.08	0.12 ± 0.06
		CCCs	23	-1.87 ± 0.52	0.66 ± 0.10	0.09 ± 0.04	0.85 ± 0.07	0.14 ± 0.06
	C07	NCCCs	24	-0.83 ± 0.58	0.83 ± 0.11	0.25 ± 0.09	1.01 ± 0.11	0.25 ± 0.10
		CCCs	23	0.82 ± 0.07	0.02 ± 0.01	-1.07 ± 0.34	0.82 ± 0.04	0.03 ± 0.02
MaxSN	Z13	NCCCs	28	-0.87 ± 0.49	0.79 ± 0.10	0.23 ± 0.08	1.20 ± 0.13	0.26 ± 0.09
		CCCs	27	-1.42 ± 0.52	0.73 ± 0.10	0.11 ± 0.04	0.94 ± 0.08	0.13 ± 0.05
	C07	NCCCs	29	-1.02 ± 0.60	0.76 ± 0.12	0.30 ± 0.10	1.19 ± 0.14	0.34 ± 0.11
		CCCs	26	-1.12 ± 0.39	0.79 ± 0.08	0.05 ± 0.02	0.94 ± 0.06	0.07 ± 0.03
NEAREST	Z13	NCCCs	28	-0.54 ± 0.49	0.88 ± 0.10	0.20 ± 0.07	1.09 ± 0.10	0.20 ± 0.07
		CCCs	27	-1.33 ± 0.52	0.74 ± 0.10	0.11 ± 0.04	0.97 ± 0.08	0.13 ± 0.05
	C07	NCCCs	29	-0.84 ± 0.57	0.81 ± 0.11	0.27 ± 0.09	1.14 ± 0.12	0.28 ± 0.09
		CCCs	26	-0.78 ± 0.36	0.86 ± 0.07	0.04 ± 0.02	0.89 ± 0.05	0.04 ± 0.02

Table 4 $Y_{\mathrm{SZ},Planck} - Y_{\mathrm{SZ},XMM}$ Scaling Relations for CCCs and NCCCs with Different $Y_{\mathrm{SZ},Planck}$ under the C07 Criterion

Class.	$Y_{\mathrm{SZ},Planck}$	Sample	N	A	B	σ_{ins}	$Y_{\mathrm{SZ},Planck}/Y_{\mathrm{SZ},XMM}$	$\sigma_{\mathrm{ins}\,|\,B=1}$
C07	[a] p2011XI	NCCCs	15	-1.40 ± 0.92	0.67 ± 0.18	0.13 ± 0.07	1.28 ± 0.14	0.14 ± 0.08
		CCCs	10	-0.23 ± 0.75	0.98 ± 0.15	0.03 ± 0.03	0.86 ± 0.06	0.02 ± 0.03
	[b] PSZ1:Y_{z}	NCCCs	29	-1.06 ± 0.45	0.75 ± 0.09	0.15 ± 0.06	1.20 ± 0.11	0.19 ± 0.07
		CCCs	23	-0.94 ± 0.46	0.83 ± 0.09	0.06 ± 0.03	0.90 ± 0.06	0.06 ± 0.03
	[c] PSZ2:blind	NCCCs	29	-0.66 ± 0.52	0.75 ± 0.10	0.21 ± 0.07	1.81 ± 0.19	0.25 ± 0.09
		CCCs	26	-0.54 ± 0.57	0.89 ± 0.11	0.11 ± 0.04	1.03 ± 0.08	0.10 ± 0.04

[a] Planck Collaboration et al. (2011c); [b] Planck Collaboration et al. (2014); [c] Planck Collaboration et al. (2016b).

Table 5 $Y_{\mathrm{SZ},Planck} - Y_{\mathrm{X}}$ Scaling Relations for CCCs and NCCCs in the NEAREST Subsample with Two Cool-core Classification Criteria

Class.	Sample	N	A	B	σ_{ins}	$Y_{\mathrm{SZ},Planck}/Y_{\mathrm{X}}$	$\sigma_{\mathrm{ins}\,|\,B=1}$
Z13	NCCCs	28	-0.75 ± 0.54	0.87 ± 0.11	0.29 ± 0.09	0.92 ± 0.10	0.29 ± 0.09
	CCCs	27	-1.62 ± 0.55	0.69 ± 0.11	0.16 ± 0.05	0.92 ± 0.08	0.20 ± 0.06
C07	NCCCs	29	-1.27 ± 0.58	0.74 ± 0.12	0.36 ± 0.11	0.99 ± 0.12	0.41 ± 0.12
	CCCs	26	-0.60 ± 0.40	0.91 ± 0.08	0.07 ± 0.03	0.84 ± 0.05	0.06 ± 0.02

profile 5000 times, following Gaussian distributions with their own uncertainties. Then the uncertainty of $Y_{\mathrm{SZ},XMM}$ is obtained.

3 RESULTS AND DISCUSSION

3.1 Fitting Method

Emcee is the affine-invariant ensemble sampler for Markov chain Monte Carlo (MCMC) designed for Bayesian parameter estimation (Foreman-Mackey et al. 2013, the code can be downloaded at `http://dan.iel.fm/emcee/current/`). We employ emcee to fit the $Y_{\mathrm{SZ,CMB}} - Y_{\mathrm{SZ,X-ray}}$ scaling relation in the linear form

$$Y = B \cdot X + A \,, \tag{6}$$

where A and B are estimated parameters, and X and Y denote the base-10 logarithm of $Y_{\mathrm{SZ,X-ray}}$ and $Y_{\mathrm{SZ,CMB}}$ ($\log_{10} Y_{\mathrm{SZ,X-ray}}$, $\log_{10} Y_{\mathrm{SZ,CMB}}$), respectively. The likelihood adopted in these fits is from equation (35) of Hogg

Table 6 Cluster Properties

Name	RA	Dec	z	θ_{500}	$Y_{SZ,Planck}$ MaxSN	$Y_{SZ,Planck}$ NEAREST	$Y_{SZ,XMM}$	Cool Core Z13	Cool Core C07
	(deg)	(deg)		(arcmin)	$(10^{-4}\ \mathrm{arcmin}^2)$	$(10^{-4}\mathrm{arcmin}^2)$	$(10^{-4}\ \mathrm{arcmin}^2)$		
2A0335	54.670	9.975	0.0347	22.4 ± 0.2	88.0 ± 8.1	91.0 ± 10.5	71.7 ± 11.5	√	√
A0085	10.459	−9.305	0.0555	14.8 ± 0.2	88.4 ± 5.0	87.7 ± 4.8	90.7 ± 7.7	√	√
A0119	14.076	−1.205	0.0444	11.6 ± 0.8	104.7 ± 11.5	104.7 ± 11.5	29.6 ± 8.6	×	×
A0133	15.675	−21.872	0.0569	16.2 ± 1.5	80.4 ± 5.8	44.5 ± 3.9	34.0 ± 7.1	√	√
A0399	44.457	13.049	0.0722	18.3 ± 0.4	135.1 ± 10.2	45.4 ± 4.3	84.3 ± 27.2	×	×
A0401	44.740	13.579	0.0739	15.1 ± 0.2	90.0 ± 6.8	90.0 ± 6.8	113.6 ± 12.3	×	×
A0478	63.356	10.467	0.0882	11.2 ± 0.4	75.1 ± 5.1	75.1 ± 5.1	111.9 ± 7.4	√	√
A0496	68.410	−13.255	0.0326	23.0 ± 0.8	98.8 ± 7.1	87.7 ± 6.5	87.1 ± 10.9	√	√
A0576	110.343	55.786	0.0381	15.7 ± 0.4	46.7 ± 5.4	53.9 ± 5.5	28.5 ± 5.8	√	×
A0644	124.355	−7.516	0.0704	15.5 ± 0.6	82.8 ± 4.9	77.9 ± 4.0	138.8 ± 19.6	√	√
A0754	137.285	−9.655	0.0542	21.0 ± 2.5	213.2 ± 15.2	202.9 ± 15.2	89.8 ± 21.2	×	×
A1413	178.827	23.407	0.1427	8.6 ± 0.3	28.2 ± 2.1	28.2 ± 2.1	36.4 ± 4.4	×	√
A1644	194.291	−17.405	0.0473	16.0 ± 1.4	54.0 ± 5.8	54.0 ± 5.8	73.4 ± 12.0	√	×
A1650	194.671	−1.755	0.0845	10.7 ± 0.1	51.2 ± 3.5	51.2 ± 3.5	53.6 ± 6.6	√	×
A1651	194.840	−4.188	0.0845	10.6 ± 0.2	45.2 ± 3.5	47.0 ± 4.0	57.8 ± 5.7	×	√
A1689	197.875	−1.338	0.1832	7.5 ± 0.4	40.2 ± 2.2	37.4 ± 1.9	34.3 ± 4.4	×	√
A1775	205.474	26.372	0.0724	9.5 ± 0.1	16.5 ± 2.6	16.5 ± 2.6	18.7 ± 1.6	√	×
A1795	207.221	26.596	0.0622	19.3 ± 0.1	87.3 ± 7.7	87.3 ± 7.7	121.3 ± 10.8	√	√
A1914	216.507	37.827	0.1712	6.3 ± 0.3	38.7 ± 3.3	26.0 ± 1.6	35.8 ± 3.0	×	√
A2029	227.729	5.720	0.0766	11.5 ± 0.5	91.5 ± 11.8	111.0 ± 11.8	119.3 ± 10.8	√	√
A2063	230.772	8.602	0.0358	15.7 ± 0.5	38.7 ± 5.2	38.7 ± 5.2	27.4 ± 6.5	×	√
A2065	230.611	27.709	0.0723	11.0 ± 0.2	42.6 ± 3.1	65.5 ± 4.8	50.2 ± 6.7	√	×
A2142	239.586	27.227	0.0894	11.0 ± 0.5	117.2 ± 15.1	156.9 ± 15.1	93.8 ± 20.2	√	√
A2163	243.945	−6.138	0.2030	12.2 ± 0.3	145.5 ± 9.1	145.5 ± 9.1	199.4 ± 40.4	×	×
A2199	247.158	39.549	0.0299	22.8 ± 0.3	110.8 ± 7.5	114.3 ± 6.6	124.6 ± 51.4	√	√
A2204	248.194	5.571	0.1514	8.6 ± 0.3	44.9 ± 2.8	41.7 ± 2.9	62.3 ± 10.3	√	√
A2255	258.197	64.061	0.0809	10.8 ± 1.0	74.7 ± 8.5	74.7 ± 8.5	41.0 ± 10.7	×	×
A2256	255.953	78.644	0.0581	13.8 ± 0.4	111.8 ± 8.5	111.8 ± 8.5	74.0 ± 10.3	×	×
A2319	290.298	43.948	0.0564	21.3 ± 0.2	273.5 ± 32.9	247.6 ± 32.9	88.0 ± 32.7	×	×
A2589	350.987	16.775	0.0416	16.0 ± 0.4	57.0 ± 12.2	31.6 ± 5.7	38.0 ± 3.6	×	√
A2597	351.333	−12.122	0.0852	7.5 ± 0.1	11.3 ± 2.4	9.8 ± 2.3	8.5 ± 2.9	√	√
A2657	356.238	9.198	0.0400	17.3 ± 1.1	33.6 ± 5.0	33.6 ± 5.0	31.5 ± 10.4	√	√
A2734	2.836	−28.855	0.0620	11.4 ± 0.6	42.6 ± 4.2	42.6 ± 4.2	26.4 ± 6.0	√	×
A3112	49.494	−44.238	0.0752	11.8 ± 0.2	28.7 ± 3.2	35.2 ± 3.4	39.2 ± 2.6	√	√
A3158	55.725	−53.638	0.0590	12.6 ± 0.4	50.0 ± 12.2	50.0 ± 12.2	47.7 ± 5.0	×	×
A3266	67.850	−61.438	0.0589	19.6 ± 1.0	173.5 ± 16.7	161.1 ± 16.7	199.1 ± 51.4	×	×
A3391	96.595	−53.688	0.0514	17.9 ± 0.7	48.9 ± 6.3	48.9 ± 6.3	48.5 ± 16.5	×	×
A3526	192.200	−41.305	0.0114	54.9 ± 0.7	211.8 ± 33.0	211.8 ± 33.0	287.9 ± 21.1	√	√
A3532	194.320	−30.372	0.0554	11.5 ± 0.9	68.5 ± 5.2	87.4 ± 6.3	35.9 ± 8.2	×	×
A3558	201.990	−31.505	0.0488	14.5 ± 0.9	36.9 ± 2.3	36.9 ± 2.3	113.9 ± 17.9	√	×
A3562	203.401	−31.655	0.0490	14.6 ± 0.3	159.8 ± 21.0	98.5 ± 12.3	32.6 ± 3.1	×	×
A3571	206.868	−32.838	0.0391	22.4 ± 0.6	163.0 ± 9.1	163.0 ± 9.1	236.0 ± 22.0	×	√
A3667	303.127	−56.822	0.0556	18.0 ± 0.3	178.3 ± 19.8	178.3 ± 19.8	246.5 ± 8.8	×	×
A3695	308.700	−35.805	0.0894	9.3 ± 0.4	19.3 ± 3.6	30.0 ± 3.9	27.4 ± 5.1	×	×
A3822	328.538	−57.855	0.0760	8.2 ± 0.7	11.1 ± 2.9	11.1 ± 2.9	17.3 ± 3.8	×	×
A3827	330.483	−59.938	0.0980	10.2 ± 0.2	48.3 ± 2.5	48.3 ± 2.5	51.8 ± 5.0	×	×
A3888	338.629	−37.738	0.1510	6.3 ± 0.8	47.7 ± 4.0	27.5 ± 1.9	27.6 ± 3.2	×	×
A4038	356.930	−28.138	0.0300	19.7 ± 0.8	42.2 ± 4.8	42.2 ± 4.8	47.9 ± 2.9	√	√
A4059	359.260	−34.755	0.0475	14.7 ± 0.2	70.7 ± 6.0	70.7 ± 6.0	59.3 ± 9.2	√	√
AWM7	43.623	41.578	0.0172	36.7 ± 1.4	202.6 ± 12.8	202.6 ± 12.8	153.8 ± 52.1	√	√
Coma	194.929	27.939	0.0231	51.8 ± 2.1	1019.5 ± 43.7	1519.1 ± 43.7	1210. ± 440.	×	×
MKW3s	230.458	7.709	0.0442	16.3 ± 1.0	30.9 ± 5.5	50.1 ± 13.0	34.0 ± 4.7	√	√
RXCJ2344.2–0422	356.067	−4.372	0.0786	8.5 ± 0.3	27.1 ± 3.1	20.4 ± 2.9	21.2 ± 4.1	×	×
S0636	157.515	−35.309	0.0116	30.9 ± 2.1	84.2 ± 12.1	84.2 ± 12.1	25.5 ± 12.9	√	×
Triangulum	249.576	−64.356	0.0510	21.2 ± 0.8	244.1 ± 50.3	244.1 ± 50.3	387.0 ± 68.7	×	×
A1835	210.260	2.880	0.2528	5.2 ± 0.3	23.4 ± 1.5	23.4 ± 1.5	23.5 ± 5.2	√	-
A2034	227.549	33.515	0.1130	7.9 ± 0.3	37.8 ± 4.3	30.8 ± 2.0	24.3 ± 3.2	×	-
A2219	250.089	46.706	0.2280	5.9 ± 0.2	42.2 ± 5.3	42.2 ± 5.3	45.0 ± 6.7	×	-
A2390	328.398	17.687	0.2329	6.5 ± 0.3	33.2 ± 1.9	47.9 ± 3.8	64.8 ± 6.6	√	-
A2420	332.582	−12.172	0.0846	13.7 ± 0.4	50.6 ± 3.3	47.5 ± 3.3	58.9 ± 12.3	×	-
A2426	333.636	−10.372	0.0980	9.7 ± 0.3	40.8 ± 5.0	25.8 ± 3.1	13.5 ± 2.2	×	-
A2626	354.126	21.142	0.0565	12.9 ± 0.5	48.4 ± 19.2	48.4 ± 19.2	15.2 ± 1.8	√	-
A3186	58.095	−74.014	0.1279	7.1 ± 0.6	30.5 ± 5.3	30.5 ± 5.3	34.1 ± 7.7	×	-
A3404	101.372	−54.222	0.1644	10.6 ± 0.3	53.5 ± 5.6	53.5 ± 5.6	60.0 ± 26.1	√	-
A3911	341.577	−52.722	0.0965	11.4 ± 0.7	34.8 ± 2.8	34.8 ± 2.8	33.9 ± 7.7	×	-
RXCJ0413.9–3805	63.488	−38.088	0.0501	14.3 ± 0.2	22.3 ± 3.8	22.3 ± 3.8	9.5 ± 2.1	×	-
RXCJ1504.1–0248	226.032	−2.805	0.2153	5.2 ± 0.1	12.4 ± 2.3	11.9 ± 2.2	18.7 ± 3.8	√	-
RXCJ1558.3–1410	239.597	−14.172	0.0970	7.6 ± 0.3	15.5 ± 3.4	15.5 ± 3.4	12.7 ± 1.7	√	-
RXCJ1720.1+2637	260.039	26.627	0.1644	6.9 ± 0.2	22.4 ± 2.3	19.1 ± 2.0	28.2 ± 3.9	√	-
RXCJ2014.8–2430	303.707	−24.505	0.1612	6.5 ± 0.4	12.1 ± 2.0	12.1 ± 2.0	23.3 ± 6.4	√	-
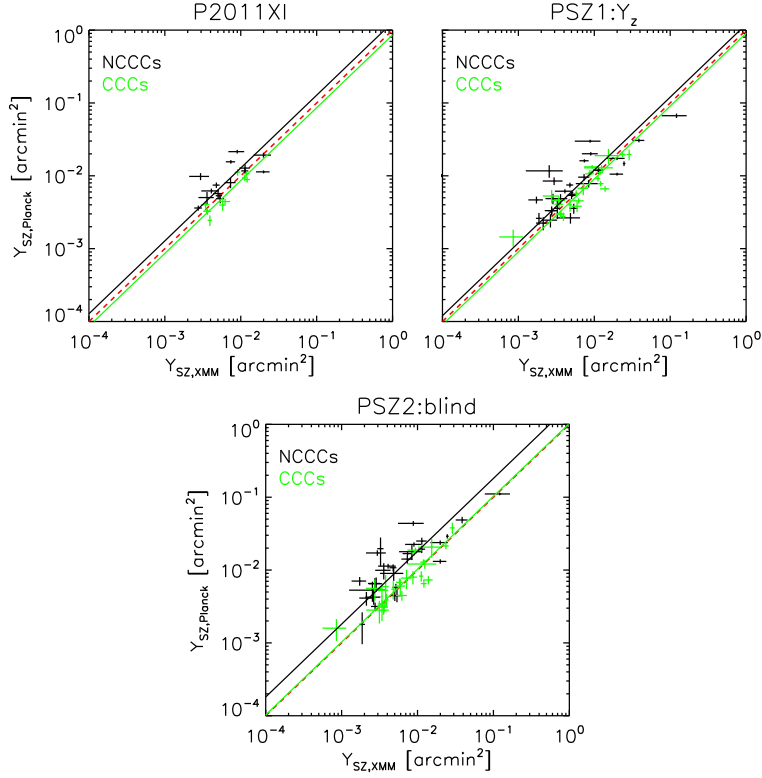
Fig. 4 $Y_{\mathrm{SZ},Planck} - Y_{\mathrm{SZ},XMM}$ scaling relations for CCCs and NCCCs with different $Y_{\mathrm{SZ},Planck}$ under the C07 criterion.
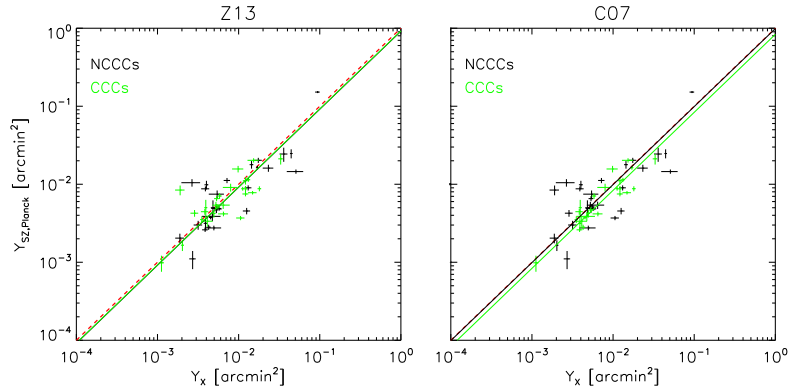
Fig. 5 $Y_{\mathrm{SZ},Planck} - Y_{\mathrm{X}}$ scaling relations for CCCs and NCCCs in the NEAREST subsample. The convention for lines and panels is the same as in Fig. 3.

et al. (2010), following Planck Collaboration et al. (2016b),

$$\ln L = -\frac{1}{2} \sum_{i=1}^{N} \left(\ln(\sigma_i^2 + \sigma_{\mathrm{int}}^2) + \sum_{i=1}^{N} \frac{(Y_i - B \cdot X_i - A)^2}{\sigma_i^2 + \sigma_{\mathrm{int}}^2} \right) ,$$
(7)

where $\sigma_i^2 = \sigma_{Y_i}^2 + B^2 \cdot \sigma_{X_i}^2$. N is the number of clusters, σ_{int} is the intrinsic scatter, and σ_{X_i} and σ_{Y_i} are statistical errors in X_i and Y_i respectively. Three parameters, A, B and σ_{int}, are estimated in the fitting procedure. We also fix

$B = 1$, and repeat the procedure above to obtain A and $\sigma_{\mathrm{ins} \mid B=1}$. The ratio of $Y_{\mathrm{SZ,CMB}}/Y_{\mathrm{SZ,X-ray}}$ equals 10^A.

3.2 $Y_{\mathrm{SZ},Planck}$ versus $Y_{\mathrm{SZ},XMM}$

$Y_{\mathrm{SZ},Planck}$ and $Y_{\mathrm{SZ},XMM}$ are all integrated within R_{500}. We construct five samples named MMF1, MMF3, PsW, MaxSN and NEAREST. $Y_{\mathrm{SZ},Planck}$ in the MMF1, MMF3 and PsW samples is given by the three corresponding

Planck extraction algorithms, fixing θ_s in the (Y_{5R500}, θ_s) probability distribution plane at the X-ray θ_s. Four clusters are discarded from the PsW sample because the X-ray θ_s is beyond the scope of the PsW (Y_{5R500}, θ_s) plane. Planck Collaboration et al. (2016b) demonstrated that the detection characteristics made by the three algorithms are consistent with each other by simulation. In order to construct a larger sample, we utilize them to build the MaxSN and NEAREST samples. In the MaxSN sample, the $Y_{SZ,Planck}$ of each cluster is assigned by the algorithm which gives the maximum S/N value, while in the NEAREST sample, the $Y_{SZ,Planck}$ of each cluster is set by the algorithm whose output position is closest to the X-ray center. With the accurately de-projected temperature and density distributions, we calculate $Y_{SZ,XMM}$ correcting the impacts of the center offsets between *XMM-Newton* and the three *Planck* algorithms. The cluster properties are listed in Table 6. Differences between $Y_{SZ,XMM}$ in the MaxSN and NEAREST samples are less than 2%, therefore we only present $Y_{SZ,XMM}$ in the NEAREST sample in this table.

The scaling relations between $Y_{SZ,Planck}$ and $Y_{SZ,XMM}$ are shown in Figure 2. The best-fitting parameters and the number of clusters for each sample are presented in Table 1. Firstly, we compare the MMF1, MMF3 and PsW samples, which are constructed by three independent detection algorithms. On the condition that the slope and normalization are free parameters, the $Y_{SZ,Planck} - Y_{SZ,XMM}$ relations in these three samples agree with each other. The intrinsic scatter in the MMF1 sample is relatively larger than that in the other algorithms. When we consider the relation with slope fixed to 1 ($B = 1$), the ratio of $Y_{SZ,Planck}/Y_{SZ,XMM}$ for the MMF1 sample is significantly higher ($\sim 4\sigma$) than that of the MMF3 and PsW samples. This is due to the different background estimations and extraction strategies in the different algorithms. For the combined samples, MaxSN and NEAREST, the $Y_{SZ,Planck} - Y_{SZ,XMM}$ relations between them are consistent. We regard the NEAREST sample as our reference sample, because the detection significance in each algorithm is different between the blind mode and the mode with a prior known cluster position, and the detection method which provides the position closest to the cluster's X-ray center is considered to be the most accurate.

The NEAREST sample contains 70 clusters, in which 18, 18 and 34 detections are respectively made by algorithms MMF1, MMF3 and PsW, confirming that PsW produces the most accurate positions (Planck Collaboration et al. 2016b). The intercept and slope of the $Y_{SZ,Planck} - Y_{SZ,XMM}$ relations in this sample are $A = -0.86 \pm 0.30$ and $B = 0.83 \pm 0.06$ respectively. The

intrinsic scatter is $\sigma_{\text{ins}} = 0.14 \pm 0.03$. The ratio of $Y_{SZ,Planck}/Y_{SZ,XMM}$ is 1.03 ± 0.05 which is in excellent statistical agreement with unity. Our results indicate that the SZ signals detected by CMB and by X-ray observations are fully consistent.

There are two papers that study the $Y_{SZ,CMB} - Y_{SZ,X-ray}$ scaling relation. Bonamente et al. (2012) present a sample of 25 massive relaxed galaxy clusters observed by the Sunyaev-Zel'dovich Array (SZA) and *Chandra*. They assume the ICM model which is introduced by Bulbul et al. (2010). This model can be applied simultaneously to SZ and X-ray data. Their ratio of $Y_{SZ,CMB}/Y_{SZ,X-ray}$ is 1.06 ± 0.04, which is in good agreement with our results. De Martino & Atrio-Barandela (2016) use a sample of 560 clusters whose properties are derived from *Planck* 2013 foreground cleaned nominal maps and *ROSAT* observations, to determine the SZ/X-ray scaling relations.

They calculate the angular size weighted Y_{SZ}, and obtain the relation $\bar{Y}_{SZ,Planck} = 0.97 \bar{Y}_{SZ,X-ray}$, which also agrees with ours.

The intrinsic scatter in our results $\sigma_{\text{ins}} = 0.14 \pm 0.03$ is slightly larger than the prediction ($\sim 10\%$). The extrapolation in both *Planck* and *XMM-Newton* may induce scatter or bias to our results. When determining $Y_{SZ,Planck}$, Y_{500} is obtained from Y_{5R500}. The shape of the GNFW pressure profile employed in the *Planck* analysis is fixed, which leaves a negligible impact on the scaling relation (Planck Collaboration et al. 2011c), but different shapes of pressure profile may have significantly different conversion factors from Y_{5R500} to Y_{500} (Sayers et al. 2016). To be more specific, each cluster has a unique pressure profile and a unique conversion factor, and converting Y_{500} from Y_{5R500} by a unified factor may induce scatter. In the extrapolation of cluster properties from X-rays, a flat temperature extending from $\sim 0.5R_{500}$ to the cluster's outer region could overestimate $Y_{SZ,XMM}$.

We also calculate the $Y_{SZ,XMM}$ whose $n_e(r)$ is fitted with only the single β model. The resulting ratio is $Y_{SZ,Planck}/Y_{SZ,XMM} = 0.89 \pm 0.05$, deviating nearly 3σ from our previous result. Many studies argue that the isothermal β model is inadequate to fit ICM and may overestimate the SZ signal (Lieu et al. 2006; Bielby & Shanks 2007; Hallman et al. 2007; Atrio-Barandela et al. 2008; Mroczkowski et al. 2009; Allison et al. 2011). Assuming two components in the ICM when fitting the electron distribution, the double β model works well within R_{500} (Chen et al. 2007).

3.3 Cool Core Influences

We construct a subsample including 55 clusters, which are overlapping clusters between the HIFLUGCS and ours. In this subsample, we refer to data in the NEAREST sample to investigate the cool core influences on the scaling relations. We adopt two methods to distinguish CCCs from NCCCs using X-ray data. The first method follows the definition in Zhao et al. (2013) (hereafter Z13): clusters with a central cooling time $t_c < 7.7h_{70}^{-1/2}$ (Rafferty et al. 2006) and a temperature drop larger than 30% from the peak are classified as CCCs. This divides the sample into 28 NCCCs and 27 CCCs. The second method follows the definition in Chen et al. (2007) (hereafter C07): clusters with significant classical mass deposition rate $\dot{M} \geq 0.01\,M_\odot\,\mathrm{yr}^{-1}$ are classified as CCCs. Instead of calculating the mass deposition rate by ourselves, we directly use their classification which divides the sample into 29 NCCCs and 26 CCCs.

Figure 3 displays the CCCs' and NCCCs' scaling relations between $Y_{\mathrm{SZ},Planck}$ and $Y_{\mathrm{SZ},XMM}$. The best-fit parameters for each subsample are presented in Table 2.

In the Z13 classification criteria, intrinsic scatter in the $Y_{\mathrm{SZ},Planck} - Y_{\mathrm{SZ},XMM}$ scaling relation of CCCs (~ 0.11) is slightly smaller than that of NCCCs (~ 0.20), and the $Y_{\mathrm{SZ},Planck}/Y_{\mathrm{SZ},XMM}$ ratio of CCCs tends to be less than that of NCCCs. Due to the relatively large uncertainties, we observe weak evidence for the discrepancies between CCCs and NCCCs. Under the C07 criteria, disagreements between CCCs and NCCCs become more significant, especially for the intrinsic scatter which is ~ 0.04 and ~ 0.28 for CCCs and NCCCs, respectively. These results are not only obtained in the NEAREST sample, they remain the same in other samples, which are shown in Table 3.

To validate our results, we use $Y_{\mathrm{SZ},Planck}$ taken from three papers, Y_{500} in Planck Collaboration et al. (2011c), Y_z in the PSZ1 catalog (Planck Collaboration et al. 2014) and Y_{blind} in the PSZ2 catalog (Planck Collaboration et al. 2016b), to discuss the cool-core influences on the $Y_{\mathrm{SZ},Planck} - Y_{\mathrm{SZ},XMM}$ scaling relations. Y_{500} in Planck Collaboration et al. (2011c) is obtained by algorithm re-extraction from *Planck* maps at the X-ray position and with the X-ray size. Y_z in PSZ1 is calculated using redshift information. Y_{blind} in PSZ2 is the blind detection which has high average bias because of the overestimated size. Our $Y_{\mathrm{SZ},Planck} - Y_{\mathrm{SZ},XMM}$ is derived from Y_{blind} restricting by our X-ray size. Under C07 cool-core criteria, CCCs and NCCCs show clear discrepancies in the SZ and X-ray measurements no matter which $Y_{\mathrm{SZ},Planck}$ we used. The results are listed in Table 4 and displayed in Figure 4.

We also examine the $Y_{\mathrm{SZ},Planck} - Y_{\mathrm{X}}$ scaling relation. Compared with $Y_{\mathrm{SZ},XMM}$, which requires accurate temperature and electron number density distribution, Y_{X}, which is equal to the mean temperature multiplied by the gas mass, is much easier to obtain. Therefore the $Y_{\mathrm{SZ},Planck} - Y_{\mathrm{X}}$ scaling relation is more widely used in comparing SZ and X-ray data. Here we define $Y_{\mathrm{X}} = T_{\mathrm{X}} \cdot M_{\mathrm{gas}} \cdot (D_{\mathrm{A}}^{-2}(\sigma_{\mathrm{T}}/m_e c^2)/(\mu_e m_{\mathrm{p}}))$, where T_{X} is the volume average temperature determined within the region $[0.2, 0.5]R_{500}$, M_{gas} is the gas mass within R_{500}, $4\pi m_{\mathrm{p}} \int_0^{R_{500}} n_e(r) r^2 dr$, with m_{p} the proton mass and μ_e the mean molecular weight of the electrons, and the factor $D_{\mathrm{A}}^{-2}(\sigma_{\mathrm{T}}/m_e c^2)/(\mu_e m_{\mathrm{p}})$ is used to convert the unit from Mpc^2 to arcmin^2.

$Y_{\mathrm{SZ},Planck} - Y_{\mathrm{X}}$ relations, with C07 and Z13 criteria, are shown in Figure 5. We find similar results in the $Y_{\mathrm{SZ},Planck} - Y_{\mathrm{X}}$ relation as in the $Y_{\mathrm{SZ},Planck} - Y_{\mathrm{SZ},XMM}$ relation, which indicate that SZ and X-ray observations of CCCs and NCCCs are inconsistent, although discrepancies in the Y-ratio between CCCs and NCCCs in the $Y_{\mathrm{SZ},Planck} - Y_{\mathrm{X}}$ relation are smaller than those in the $Y_{\mathrm{SZ},Planck} - Y_{\mathrm{SZ},XMM}$ relation. Intrinsic scatters of CCCs and NCCCs still significantly disagree with each other. The results are listed in Table 5. We emphasize that $Y_{\mathrm{SZ},Planck}/Y_{\mathrm{X}} = 0.92 \pm 0.05$ is completely consistent with the prediction in X-ray, 0.924 ± 0.004 (Arnaud et al. 2010).

Our sample is an intersection of the X-ray sample with flux limit, and the *Planck* sample with S/N cut. The selection effects of the Malmquist bias (Stanek et al. 2006) and Eddington bias (Maughan 2007) may cause the results to deviate due to scatters in these scaling relations around the limit/cut. To quantify these effects on scaling relations, complicated computations are required to generate a large mock cluster sample from the assumed mass function, to mimic the observed sample with the same selection criteria (Vikhlinin et al. 2009a; Planck Collaboration et al. 2011a,c; Rozo et al. 2012; Czakon et al. 2015; De Martino & Atrio-Barandela 2016). For the Y-ratio, the correction is negligible according to Planck Collaboration et al. (2011c); Rozo et al. (2012); Czakon et al. (2015); De Martino & Atrio-Barandela (2016). The bias should be fairly small for very luminous objects (Planck Collaboration et al. 2011b; Rozo et al. 2012; Planck Collaboration et al. 2016b). As the galaxy clusters in our sample are very bright clusters with strong SZ detections, we believe the bias of the Eddington effect and Malmquist effect is fairly small in our $Y_{\mathrm{SZ},Planck} - Y_{\mathrm{SZ},XMM}$ scaling relation. The discrepancies between CCCs and NCCCs are due to other reasons. However, we should also bear in mind that our

$Y_{\mathrm{SZ},Planck} - Y_{\mathrm{SZ},XMM}$ scaling relation is derived from the most luminous clusters. Applications to dimmer clusters with this scaling relation should be considered carefully.

Most CCCs are relaxed systems while NCCCs are undergoing more disturbing processes, like merging. Therefore, the intrinsic scatter of CCCs is smaller than that of NCCCs. The ratio of $Y_{\mathrm{SZ},Planck}/Y_{\mathrm{SZ},XMM}$ in CCCs (NCCCs) has a trend to be smaller (larger) than unity, which implies that the outskirt pressure profiles of CCCs and NCCCs could have substantial differences, instead of following a universal profile.

Because of the different dynamical states of CCCs and NCCCs, it is natural to believe that the $Y_{\mathrm{SZ,CMB}} - Y_{\mathrm{SZ,X-ray}}$ scaling relation of CCCs and NCCCs could have discrepancies, but previous measurements show little difference between them (Planck Collaboration et al. 2013b; Rozo et al. 2012; De Martino & Atrio-Barandela 2016). This contradiction may be mainly due to our high quality X-ray data. We processed the *XMM-Newton* data in detail, and no scaling relation was adopted during the data analysis. Another reason may be due to the cool-core classification criteria. In our results, the CCC and NCCC discrepancies are more significant with the C07 definition, therefore the mass deposition rate may be much closer to the physical nature of CCCs and NCCCs than the central gas density, core entropy excess and central cooling time, which previous works apply to distinguish CCCs from NCCCs.

4 CONCLUSIONS

In this paper we use a sample of 70 clusters to study the $Y_{\mathrm{SZ},Planck} - Y_{\mathrm{SZ},XMM}$ scaling relations and compare the differences between CCCs and NCCCs. The $Y_{\mathrm{SZ},XMM}$ is calculated by accurately de-projected temperature and electron number density profiles derived from *XMM-Newton*, with correction for the cluster center offset between two satellites, and the $Y_{\mathrm{SZ},Planck}$ is the latest *Planck* data restricted to our X-ray cluster size θ_{500}. We build five samples: MMF1, MMF3, PsW, MaxSN and NEAREST, with the MaxSN and NEAREST samples being combinations of MMF1, MMF3 and PsW.

The results in the MaxSN and NEARESET samples are in full agreement, and we choose the NEAREST sample as our reference. The intercept and slope of the $Y_{\mathrm{SZ},Planck} - Y_{\mathrm{SZ},XMM}$ scaling relation are $A = -0.86 \pm 0.30$ and $B = 0.83 \pm 0.06$ respectively. The intrinsic scatter is $\sigma_{\mathrm{ins}} = 0.14 \pm 0.03$. The ratio of $Y_{\mathrm{SZ},Planck}/Y_{\mathrm{SZ},XMM}$ is 1.03 ± 0.05, which is in excellent statistical agreement with unity.

We use two classification criteria to distinguish CCCs from NCCCs. Both criteria indicate that the properties of CCCs are inconsistent with those of NCCCs. The intrinsic scatter of CCCs is rather small compared with that of NCCCs, and the ratio of $Y_{\mathrm{SZ},Planck}/Y_{\mathrm{SZ},XMM}$ for CCCs (NCCCs) has a slight inclination to be smaller (larger) than unity, suggesting that $Y_{\mathrm{SZ},XMM}$ for CCCs (NCCCs) may overestimate (underestimate) the SZ signal. Discrepancies under the criterion of C07 are more significant than those under Z13. We study the $Y_{\mathrm{SZ},Planck} - Y_{\mathrm{SZ},XMM}$ relation using another $Y_{\mathrm{SZ},Planck}$ taken from three *Planck* papers, and we also investigate the $Y_{\mathrm{SZ},Planck} - Y_{\mathrm{X}}$ relation in the same way. We find that cool-cores do have an influence on the SZ/X-ray scaling relation. Therefore, we draw a firm conclusion that the intrinsic scatter and the $Y_{\mathrm{SZ},Planck}/Y_{\mathrm{SZ},XMM}$ ratio of CCCs disagree with those of NCCCs.

References

Aghanim, N., da Silva, A. C., & Nunes, N. J. 2009, A&A, 496, 637

Allen, S. W., Evrard, A. E., & Mantz, A. B. 2011, ARA&A, 49, 409

Allison, J. R., Taylor, A. C., Jones, M. E., Rawlings, S., & Kay, S. T. 2011, MNRAS, 410, 341

Andersson, K., Benson, B. A., Ade, P. A. R., et al. 2011, ApJ, 738, 48

Angulo, R. E., Springel, V., White, S. D. M., et al. 2012, MNRAS, 426, 2046

Arnaud, M., Pointecouteau, E., & Pratt, G. W. 2005, A&A, 441, 893

Arnaud, M., Pointecouteau, E., & Pratt, G. W. 2007, A&A, 474, L37

Arnaud, M., Pratt, G. W., Piffaretti, R., et al. 2010, A&A, 517, A92

Atrio-Barandela, F., Kashlinsky, A., Kocevski, D., & Ebeling, H. 2008, ApJ, 675, L57

Benson, B. A., de Haan, T., Dudley, J. P., et al. 2013, ApJ, 763, 147

Bielby, R. M., & Shanks, T. 2007, MNRAS, 382, 1196

Biffi, V., Sembolini, F., De Petris, M., et al. 2014, MNRAS, 439, 588

Bocquet, S., Saro, A., Mohr, J. J., et al. 2015, ApJ, 799, 214

Böhringer, H., Chon, G., Collins, C. A., et al. 2013, A&A, 555, A30

Böhringer, H., Voges, W., Huchra, J. P., et al. 2000, ApJS, 129, 435

Böhringer, H., Schuecker, P., Guzzo, L., et al. 2004, A&A, 425, 367

Bonamente, M., Hasler, N., Bulbul, E., et al. 2012, New Journal of Physics, 14, 025010

Bulbul, G. E., Hasler, N., Bonamente, M., & Joy, M. 2010, ApJ, 720, 1038

Chen, Y., Ikebe, Y., & Böhringer, H. 2003, A&A, 407, 41

Chen, Y., Reiprich, T. H., Böhringer, H., Ikebe, Y., & Zhang, Y.-Y. 2007, A&A, 466, 805

Colberg, J. M., White, S. D. M., Jenkins, A., & Pearce, F. R. 1999, MNRAS, 308, 593

Comis, B., de Petris, M., Conte, A., Lamagna, L., & de Gregori, S. 2011, MNRAS, 418, 1089

Czakon, N. G., Sayers, J., Mantz, A., et al. 2015, ApJ, 806, 18

De Grandi, S., Böhringer, H., Guzzo, L., et al. 1999, ApJ, 514, 148

De Martino, I., & Atrio-Barandela, F. 2016, MNRAS, 461, 3222

Ebeling, H., Edge, A. C., Bohringer, H., et al. 1998, MNRAS, 301, 881

Ebeling, H., Voges, W., Bohringer, H., et al. 1996, MNRAS, 281, 799

Foreman-Mackey, D., Hogg, D. W., Lang, D., & Goodman, J. 2013, PASP, 125, 306

Hallman, E. J., Burns, J. O., Motl, P. M., & Norman, M. L. 2007, ApJ, 665, 911

Hogg, D. W., Bovy, J., & Lang, D. 2010, arXiv:1008.4686

Jia, S.-M., Chen, Y., & Chen, L. 2006, ChJAA (Chin. J. Astron. Astrophys.), 6, 181

Jia, S. M., Chen, Y., Lu, F. J., Chen, L., & Xiang, F. 2004, A&A, 423, 65

Jimeno, P., Diego, J. M., Broadhurst, T., De Martino, I., & Lazkoz, R. 2018, MNRAS, 478, 638

Kravtsov, A. V., & Borgani, S. 2012, ARA&A, 50, 353

Kravtsov, A. V., Vikhlinin, A., & Nagai, D. 2006, ApJ, 650, 128

Lieu, R., Mittaz, J. P. D., & Zhang, S.-N. 2006, ApJ, 648, 176

Mahdavi, A., Hoekstra, H., Babul, A., et al. 2013, ApJ, 767, 116

Mantz, A., Allen, S. W., Rapetti, D., & Ebeling, H. 2010, MNRAS, 406, 1759

Maughan, B. J. 2007, ApJ, 668, 772

Mewe, R., Gronenschild, E. H. B. M., & van den Oord, G. H. J. 1985, A&AS, 62, 197

Morrison, R., & McCammon, D. 1983, ApJ, 270, 119

Motl, P. M., Hallman, E. J., Burns, J. O., & Norman, M. L. 2005, ApJ, 623, L63

Mroczkowski, T., Bonamente, M., Carlstrom, J. E., et al. 2009, ApJ, 694, 1034

Munari, E., Biviano, A., Borgani, S., Murante, G., & Fabjan, D.

2013, MNRAS, 430, 2638

Nagai, D. 2006, ApJ, 650, 538

Planck Collaboration, Ade, P. A. R., Aghanim, N., et al. 2011a, A&A, 536, A8

Planck Collaboration, Aghanim, N., Arnaud, M., et al. 2011b, A&A, 536, A10

Planck Collaboration, Ade, P. A. R., Aghanim, N., et al. 2011c, A&A, 536, A11

Planck Collaboration, Ade, P. A. R., Aghanim, N., et al. 2013a, A&A, 550, A129

Planck Collaboration, Ade, P. A. R., Aghanim, N., et al. 2013b, A&A, 550, A131

Planck Collaboration, Ade, P. A. R., Aghanim, N., et al. 2014, A&A, 571, A29

Planck Collaboration, Ade, P. A. R., Aghanim, N., et al. 2016a, A&A, 594, A24

Planck Collaboration, Ade, P. A. R., Aghanim, N., et al. 2016b, A&A, 594, A27

Pratt, G. W., Croston, J. H., Arnaud, M., & Böhringer, H. 2009, A&A, 498, 361

Reichert, A., Böhringer, H., Fassbender, R., & Mühlegger, M. 2011, A&A, 535, A4

Reiprich, T. H., & Böhringer, H. 2002, ApJ, 567, 716

Rozo, E., Evrard, A. E., Rykoff, E. S., & Bartlett, J. G. 2014a, MNRAS, 438, 62

Rozo, E., Rykoff, E. S., Bartlett, J. G., & Evrard, A. 2014b, MNRAS, 438, 49

Rozo, E., Vikhlinin, A., & More, S. 2012, ApJ, 760, 67

Rozo, E., Wechsler, R. H., Rykoff, E. S., et al. 2010, ApJ, 708, 645

Sayers, J., Golwala, S. R., Mantz, A. B., et al. 2016, ApJ, 832, 26

Seljak, U., Slosar, A., & McDonald, P. 2006, J. Cosmol. Astropart. Phys., 10, 014

Sembolini, F., De Petris, M., Yepes, G., et al. 2014, MNRAS, 440, 3520

Stanek, R., Evrard, A. E., Böhringer, H., Schuecker, P., & Nord, B. 2006, ApJ, 648, 956

Sunyaev, R. A., & Zeldovich, I. B. 1980, ARA&A, 18, 537

Vikhlinin, A., Burenin, R. A., Ebeling, H., et al. 2009a, ApJ, 692, 1033

Vikhlinin, A., Kravtsov, A. V., Burenin, R. A., et al. 2009b, ApJ, 692, 1060

XMM-Newton Users Handbook, Issue 2.16 (ESA: XMM-Newton SOC)

Zhang, Y.-Y., Andernach, H., Caretta, C. A., et al. 2011, A&A, 526, A105

Zhao, H.-H., Jia, S.-M., Chen, Y., et al. 2013, ApJ, 778, 124

Zhao, H.-H., Li, C.-K., Chen, Y., Jia, S.-M., & Song, L.-M. 2015, ApJ, 799, 47

Zhao, H.-H. 2015, The Statistical Studies on the X-ray Properties of Galaxy Clusters, PhD thesis, Institute of High Energy Physics, Chinese Academy of Science, China